Journal of Power Sources 195 (2010) 1957–1963

Contents lists available at ScienceDirect

Journal of Power Sources

journal homepage: www.elsevier.com/locate/jpowsour

Catalytic hydrolysis of ammonia borane: Intrinsic parameter estimation and validation

S. Basu[a,b,c], Y. Zheng[a,c,*], A. Varma[b,c], W.N. Delgass[b,c], J.P. Gore[a,b,c]

[a] School of Mechanical Engineering, Purdue University, West Lafayette, IN 47907-2088, USA
[b] School of Chemical Engineering, Purdue University, West Lafayette, IN 47907-2100, USA
[c] Energy Center in Discovery Park, Purdue University, West Lafayette, IN 47907-2022, USA

ARTICLE INFO

Article history:
Received 22 September 2009
Received in revised form 27 October 2009
Accepted 27 October 2009
Available online 5 November 2009

Keywords:
Ammonia borane
Catalytic hydrolysis
Kinetic parameter estimation
Mass diffusion coefficient
Packed-bed reactor model

ABSTRACT

Ammonia borane (AB) hydrolysis is a potential process for on-board hydrogen generation. This paper presents isothermal hydrogen release rate measurements of dilute AB (1 wt%) hydrolysis in the presence of carbon supported ruthenium catalyst (Ru/C). The ranges of investigated catalyst particle sizes and temperature were 20–181 μm and 26–56 °C, respectively. The obtained rate data included both kinetic and diffusion-controlled regimes, where the latter was evaluated using the catalyst effectiveness approach. A Langmuir–Hinshelwood kinetic model was adopted to interpret the data, with intrinsic kinetic and diffusion parameters determined by a nonlinear fitting algorithm. The AB hydrolysis was found to have an activation energy 60.4 kJ mol^{-1}, pre-exponential factor 1.36×10^{10} mol (kg-cat)$^{-1}$ s^{-1}, adsorption energy −32.5 kJ mol^{-1}, and effective mass diffusion coefficient 2×10^{-10} m^2 s^{-1}. These parameters, obtained under dilute AB conditions, were validated by comparing measurements with simulations of AB consumption rates during the hydrolysis of concentrated AB solutions (5–20 wt%), and also with the axial temperature distribution in a 0.5 kW continuous-flow packed-bed reactor.

1. Introduction

Safe and high density on-board storage of hydrogen for fuel cell applications is a challenge. High-pressure (40 g L^{-1} at 70 MPa, 288 K) and cryogenic (70 g L^{-1} at 21 K, 1 bar) storage of hydrogen is difficult because of low gravimetric/volumetric densities of the former and low storage temperatures of the latter [1–3]. Hence, storage of hydrogen in solid form is being pursued. Chemical hydrides such as ammonia borane (AB), sodium borohydride (SBH) [4] and calcium borohydride [5] are considered to be promising hydrogen storage materials. Among all hydrides, AB has the highest material hydrogen content (19.6 wt%). Each milliliter of AB weighs about three-quarters of a gram and contains up to 1.8 L of hydrogen at STP [6]. Under the same conditions AB pellets, weighing 240 mg each and occupying 0.32 mL, are capable of storing 0.52 L of hydrogen at STP [6]. Thermolysis [7–9] and catalytic hydrolysis mechanisms [10–16] of dehydrogenating AB are being investigated for rapid and controlled hydrogen release over a convenient temperature range. Non-catalytic dehydrogenation of AB mixtures, by combustion with metal powder-gelled water and by hydrothermolysis [17], has also been reported.

Potential large scale application of AB-based systems requires its regeneration from reaction by-products, for which methods [11,18,19] are being developed. The spent fuel of AB hydrolysis constitutes B–O bonds which are thermodynamically more stable than the B–N bonds in the spent fuel of AB thermolysis. Based upon AB regeneration experiments, the first attempted material yields were around 65% for spent fuels of AB hydrolysis [11] and thermolysis [19]. The estimated theoretical maximum energy efficiencies for the regeneration of spent fuels of AB hydrolysis and thermolysis are 46% and 65%, respectively [19]. An overall comparison and selection of a chemical storage material including mass and energy balances, equipment design, manufacturability, reliability and maintainability remain a continuing area of work.

Among hydrogen generation methods, the AB hydrolysis reaction [12–16] is being investigated actively:

$$NH_3BH_3 + 2H_2O \xrightarrow{\text{catalyst}} NH_4^+ + BO_2^- + 3H_2 \quad (1)$$

The choice of an appropriate catalyst for the reaction is important for reactor design. It dictates the hydrogen release rate and reactor weight. The kinetics of AB hydrolysis catalyzed by solid acid [12],

* Corresponding author at: School of Mechanical Engineering, Purdue University, 500 Allison Rd., West Lafayette, IN 47907-2088, USA. Tel.: +1 307 766 3905; fax: +1 307 766 2695.
E-mail addresses: basu1@purdue.edu (S. Basu), zhengy@ecn.purdue.edu, zhengy@ecn.purdue.edu (Y. Zheng), avarma@purdue.edu (A. Varma), delgass@purdue.edu (W.N. Delgass), gore@purdue.edu (J.P. Gore).

0378-7753/$ – see front matter © 2009 Elsevier B.V. All rights reserved.
doi:10.1016/j.jpowsour.2009.10.070

Nomenclature

A	pre-exponential factor in Arrhenius form of rate constant (kmol s^{-1} kg-cat^{-1})
$C_{AB,0}$	initial concentration of NH_3BH_3 (kmol m^{-3})
$C_{AB}(t)$	instantaneous concentration of NH_3BH_3 at time t (kmol m^{-3})
D_{eff}	effective diffusion coefficient inside catalyst pores (m^2 s^{-1})
D_l	bulk diffusion coefficient inside catalyst pores (m^2 s^{-1})
d_p	catalyst particle diameter (m)
E_a	activation energy for the hydrolysis reaction (kJ mol^{-1})
ΔH_{rxn}	heat of reaction of AB hydrolysis (-156 kJ mol^{-1})
k	rate constant for Langmuir–Hinshelwood kinetic model (kmol s^{-1} kg-cat^{-1})
k_{H_2O}	mass transfer coefficient for water vapor (3 m^{-1})
m_{cat}	mass of catalyst (mg)
$m_{H_2O,0}$	mass of water in AB solution at the start of hydrolysis (kg)
$n_{AB,0}$	moles of AB initially injected in the batch reactor (mol)
n_{H_2}	instantaneous moles of hydrogen produced during AB hydrolysis (mol)
P_{max}	barometric pressure inside gas burette at the end of reaction (Pa)
r_{obs}	observed initial reaction rate (mol m^{-3} min^{-1})
SLPM	standard liters per minute
T, T_{rxn}	reaction temperature (°C)
T_{ref}	reference reaction temperature (°C)
T_w	wall temperature of burette in which hydrogen collects (K)
T_0	reference temperature (25.6 °C)
t	time (s)
V_{H_2}	the instantaneous volume of H_2 collected at time t (mL)
$V_{H_2,max}$	total volume of H_2 collected at the end of reaction (mL)
V_{sol}	volume of solvent (m^3)

Greek letters

α	product of adsorption equilibrium constant and bulk concentration of AB
ρ_s	catalyst pellet density (656 kg m^{-3})
ε_S	internal void fraction of catalyst pellet
ϕ	Thiele modulus
η	catalyst effectiveness
μ_w	viscosity of water (N s m^{-2})
τ	tortuosity factor, typically 3.0–4.0

Subscripts

0	initial value
b	bulk value
s	property of catalyst pellet

and transition metal [10,11,13,14,16,20] catalysts are reported. In particular, ruthenium showed high catalytic activity [11,15,16,21], and the kinetic parameters for carbon supported Ru are reported [15]. However, the samples of AB used in the different studies [10,11–15,22] vary in purity, leading to different rates and parameters under similar reaction conditions. Hydrolysis of 90% pure AB (Sigma–Aldrich, Milwaukee, WI) was reported in Refs. [10,12–14] and that of 98% pure AB was reported in Refs. [11,15]. The AB (Aviabor, Dzerzhinsk, Nizhny Novgorod, Russia), used in the present study, had purity >99%. The differences in material purity, affecting its stability [23], are plausibly attributed to varying solvents used during AB synthesis. AB (Aviabor) was used because it is stable and commercially available, facilitating reproducibility of results.

In the present work, hydrogen evolution rates from the isothermal hydrolysis of Ru-catalyzed, dilute AB (1 wt%) were measured at batch sizes of 10 mL and temperature range 26–56 °C. The effect of internal diffusion within the catalyst particles, in these batch reactions, could not be eliminated at temperatures above 26 °C and thus, the measured rate data were apparent and not intrinsic. In such cases, the catalyst effectiveness (η), which depends on several parameters including the effective liquid phase mass diffusion coefficient (D_{eff}) [24], was determined. D_{eff} was estimated using concentration–time (C_{AB}-t) measurements at different catalyst particle sizes. The AB hydrolysis had apparent reaction order between zero and unity in the temperature range of the study. A Langmuir–Hinshelwood (LH) kinetic model was adopted to interpret the kinetic data with the parameters (activation energy, E_a, pre-exponential factor, A, adsorption energy, ΔH_{ads}, and adsorption equilibrium constant, K_0) determined using a nonlinear conjugate-gradient minimization algorithm [15].

These parameters, obtained under dilute conditions, are valuable if they can be extended to practical concentrations and continuous-flow systems. Hence, the obtained parameters were validated by comparing measurements in a batch reactor with simulations of AB hydrolysis at higher concentrations (5–20 wt%) where it is difficult to maintain constant temperature which complicates parameter estimation. The non-isothermal high-strength AB (5–20 wt%) hydrolysis was modeled using parameters obtained for the dilute strength of 1 wt%. The variations in temperature measured during the non-isothermal hydrolysis, reported in Ref. [20], were used in the simulations. In addition, the experimental studies [11–16,20] were restricted to batch sizes $\leq$10 mL. Simulating the hydrolysis in a continuous-flow reactor, using the parameters obtained under dilute conditions from the 10 mL batch reactions, is desired. Based on this consideration, a subscale AB hydrolysis reactor, packed with Ru/C pellets, was modeled. The packed-bed reactor model was similar to that developed previously for SBH hydrolysis [25]. AB hydrolysis was simulated at a flow rate of 22.4 g min^{-1}, with an inlet solution concentration of 5 wt% AB. The model calculations were compared with experimental data reported in Ref. [20].

Based on the above, the specific objectives of the present work are to:

1. obtain the effective mass diffusion coefficient (D_{eff}) of Ru-catalyzed AB hydrolysis, at different temperatures (26–56 °C), using appropriate C_{AB}-t measurements in a batch reactor under dilute conditions (1 wt% AB);
2. determine the catalyst effectiveness (η) and intrinsic kinetic parameters (A, E_a, K_0, ΔH_{ads}) for AB hydrolysis using the measured rate data at 1 wt% AB;
3. validate the kinetic and diffusion parameters by using them to model experimental data for AB hydrolysis at higher concentrations (5–20 wt%) in a batch reactor, as well as in a continuous-flow subscale (0.5 kW) packed-bed reactor.

2. Experimental

2.1. Materials, apparatus and procedure

Commercial AB (Aviabor) and 3 wt% Ru supported on cylindrical carbon pellets (2 mm diameter, 3 mm length, specific area ~1000 m^2 g^{-1}, Johnson Matthey, Oakbrook, IL), ground and sized

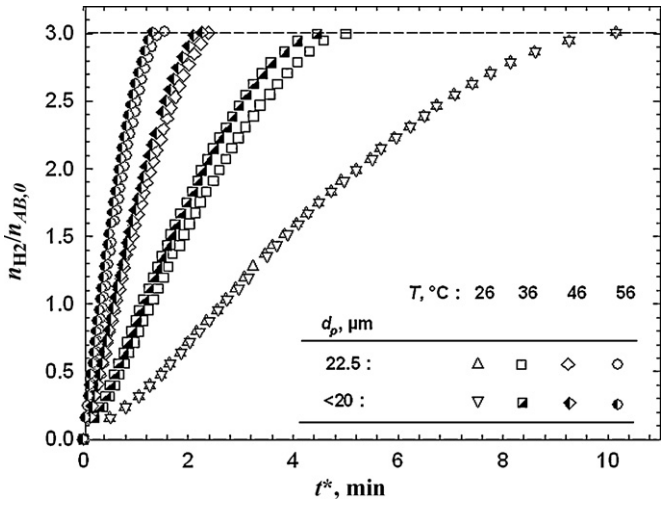

Fig. 1. AB hydrolysis at catalyst sizes of 22.5 μm and <20 μm, and temperatures 26–56 °C. The time axis was scaled as $t^* = ((m_{cat}/m^*_{cat})(n^*_{AB,0}/n_{AB,0}))t$, where m^*_{cat} = 15.2 mg, $n^*_{AB,0}$ = 2.535 mmol, $C_{AB,0}$ = 260 mol m^{-3}. Reaction conditions (T, m_{cat}, V_{sol}) at d_p = 22.5 μm were: (26 °C, 15.4 mg, 9.87 mL), (36 °C, 15.3 mg, 9.86 mL), (46 °C, 10.6 mg, 9.91 mL) and (56 °C, 6.3 mg, 9.77 mL).

prior to use, were utilized in the AB hydrolysis experiments. A schematic of the apparatus and details of the experimental procedure are reported in Ref. [15]. A 25 mL, 3-necked reaction flask was loaded with (15.2 ± 0.1) mg of the ground catalyst, 2 mL of pre-wetting water [4,15] and a magnetic stirring bead. It was submerged in a water bath and preheated to the desired reaction temperature using a thermostatic circulator. Approximately 2.53 mmol (~7.8 mL) of an AB (1 wt%) solution, prepared separately and preheated to the reaction temperature [4], were then drawn and injected into the reaction flask. The AB solution and the ground catalyst were well mixed by using a magnetic stirrer. A bayonet type-T (copper–constantan) thermocouple with a stainless steel sheath was used to record the temperature of the solution in reaction flask. The reaction temperature was controlled within ±1 °C by the thermostatic circulator. The evolved hydrogen was collected in a gas burette with a resolution of 1.0 mL. The amount of collected hydrogen in the burette was calculated using the ideal gas law with the consideration of the pressure variation caused by the change of water column height. The burette outer wall temperature, T_w, was measured to represent the accumulated hydrogen gas temperature [4].

2.2. Selection of catalyst size and stirring speed

All experiments were performed at a stirring speed of 800 rpm, chosen after the independence of kinetic performance over a range of stirring speeds from 200 to 1000 rpm confirmed that the reaction was free from external mass transfer at that speed. The effects of catalyst particle size were studied at four temperatures, 26, 36, 46 and 56 °C, in order to find a catalyst size at each temperature where the AB hydrolysis was free from internal diffusion effects as well. Fig. 1 shows the hydrogen evolution curves, for catalyst particle sizes of 22.5 μm and <20 μm, at the four temperatures studied. It may be seen from Fig. 1 that the two catalyst sizes gave the same rates only at 26 °C, thus the reactions were kinetically controlled and diffusion effects were absent at that temperature. At higher temperatures, the reaction rates did not coincide for the catalyst sizes, implying that the kinetic data obtained at these temperatures were influenced by internal diffusion. A method to obtain the intrinsic kinetic parameters using the measured rate data is presented in this work.

2.3. Experimental uncertainties

The uncertainties in the gas temperature and gas volume measurements caused ±1.08% experimental uncertainties in the mole of hydrogen collected or the mole of AB consumed. Also, random errors in time, m_{cat} and V_{sol} measurements caused ±4.6% experimental uncertainty (with 95% confidence) based upon four repeated tests under same conditions. As a result, the overall experimental uncertainties in the mole of hydrogen collected or the mole of AB consumed were estimated to be ±6.4% with 95% confidence.

3. Data analysis method

In cases where the effects of internal diffusion could not be eliminated, the governing rate equation used was based on the LH kinetic model:

$$\frac{dC_{AB}}{dt} = -\eta \frac{m_{cat}}{V_{sol}} A \exp\left(-\frac{E_a}{RT}\right) \times \frac{K_0 \exp((\Delta H_{ads}/RT_0) - (\Delta H_{ads}/RT))C_{AB}}{1 + K_0 \exp((\Delta H_{ads}/RT_0) - (\Delta H_{ads}/RT))C_{AB}} \quad (2)$$

There are five unknowns in this multiple-variable inverse problem: A, E_a, K_0, ΔH_{ads} and η, where the latter depends on D_{eff}. For each temperature and catalyst particle size (assumed to be spherical), the D_{eff} value was determined separately, yielding η, and the remaining four parameters were obtained using Eq. (2) and a nonlinear fitting procedure.

3.1. Effective mass diffusion coefficient (D_{eff})

The diffusion coefficient was determined using the $\eta - \phi$ relationship, where ϕ is the Thiele modulus [24,26–28]. The catalyst effectiveness in the diffusion-controlled regime for a spherical pellet, based on the LH model [28], depends on five parameters (A, E_a, K_0, ΔH_{ads}, D_{eff}) as shown in Eqs. (3) and (4). Eq. (3) was not directly used for D_{eff} estimation, as it is coupled to the other kinetic parameters:

$$\eta = \frac{D_{eff}(1+\alpha)}{k\rho_s(d_p/6)^2}\left[\frac{2(1+\alpha)}{\alpha}\left\{1 - \frac{1}{\alpha}\ln(1+\alpha)\right\}\right]^{1/2}, \quad (3)$$

where

$$\alpha = K_0 \exp\left(\frac{\Delta H_{ads}}{RT_0} - \frac{\Delta H_{ads}}{RT}\right) C_{AB} \quad (4)$$

However, using an nth order kinetic model was a simple and approximate method of decoupling D_{eff} from the remaining four parameters in Eq. (2), and determining them separately.

The basis of obtaining D_{eff}, using nth order kinetics, lies in identifying the two limiting regimes of reaction behavior: (a) the kinetically controlled regime and (b) the limit of strong pore-diffusion regime. The catalyst effectiveness is unity ($\eta = 1$) for small-sized catalyst particles ($\phi \to 0$) in the kinetically controlled regime, and the apparent and intrinsic rate constants are identical in such cases. On the other hand, pore-diffusion control occurs at large particle sizes, where $\phi \to \infty$ and $\eta = 1/\phi$, and the observed reaction rate is inversely proportional to the catalyst particle size [24,26]. The apparent reaction order is the same as the intrinsic value, n, in the kinetically controlled regime, whereas it is:

$$n_{obs} = \frac{n+1}{2} \quad (5)$$

in the pore-diffusion-controlled regime [26]. The Thiele modulus for an nth order reaction [24,31] is:

$$\phi = \frac{d_p}{6}\sqrt{\frac{n+1}{2}}\sqrt{\frac{k\rho_s}{D_{eff}}}\, C_{AB}^{(n-1)/2} \quad (6)$$

Based on the above-mentioned theory, the rate equations describing AB hydrolysis in the kinetically controlled and strong pore-diffusion regimes respectively were:

$$\frac{dC_{AB}}{dt} = -\eta \frac{km_{cat}}{V_{sol}} C_{AB}^{n} = -\frac{km_{cat}}{V_{sol}} C_{AB}^{n} \tag{7}$$

$$\eta = \frac{6D_{eff}}{k\rho_s d_p[((K_0 \exp((\Delta H_{ads}/RT_0) - (\Delta H_{ads}/RT))C_{AB,b})/(1 + K_0 \exp((\Delta H_{ads}/RT_0) - (\Delta H_{ads}/RT))C_{AB,b}))]} (dC_{AB}/dr)\big|_{r=(d_p/2)} \tag{13}$$

$$\frac{dC_{AB}}{dt} = -\eta \frac{km_{cat}}{V_{sol}} C_{AB}^{n} = -\left(\frac{6}{d_P}\frac{m_{cat}}{V_{sol}}\sqrt{\frac{2}{n+1}\frac{kD_{eff}}{\rho_s}}\right) C_{AB}^{(n+1)/2} \tag{8}$$

Keeping all other reaction conditions the same, AB was hydrolyzed at different catalyst particle sizes at a temperature where internal diffusion effects were absent (26 °C) at the smallest catalyst size (22.5 μm). The slopes ($d(n_{H_2}/n_{AB,0})/dt$) of the hydrogen evolution curves yielded the observed reaction rates, r_{obs}, at these catalyst sizes. The strong pore-diffusion regime was identified by verifying if the observed reaction rates were inversely proportional to the catalyst sizes as:

$$\frac{(r_{obs})_1}{(r_{obs})_2} = \frac{(d_p)_2}{(d_p)_1} \tag{9}$$

In the present work, catalyst sizes of 90.5, 128 and 181 μm were found to lie in this regime. The reaction order (n) was found by plotting the $(C_{AB,0}^{1-n} - C_{AB}^{1-n}/1-n)$ values versus time, in both the kinetically controlled (22.5 μm catalyst size) and strong pore-diffusion (90.5, 128 and 181 μm) regimes for different guessed values of n. As noted above, if the approach followed is correct, then the n value in the latter regime (n_{obs}) should be related to the intrinsic n value by Eq. (5). A unique value of n that yielded the best linear fits at these catalyst sizes was thus determined. The slope of the $(C_{AB,0}^{1-n} - C_{AB}^{1-n}/1-n)$ versus t curve, at the catalyst size in the kinetically controlled regime (22.5 μm), yielded the value of $((m_{cat}/V_{sol})k)$ obtained by integrating Eq. (7) under the assumption that n remains constant. The slope, in turn, yielded the intrinsic rate constant (k). Subsequently, the value of D_{eff} (at 26 °C) was numerically estimated using the obtained intrinsic values of n and k, and Eq. (8), along with an Euler predictor-corrector finite difference discretization. The root-mean square (rms) error between the experimental rate data obtained in the strong pore-diffusion regime and the model calculation was minimized. The intrinsic liquid phase diffusivity (D_l) was estimated from the effective diffusion coefficient as:

$$D_l = D_{eff}\frac{\tau}{\varepsilon_S}, \tag{10}$$

where ε_S and τ were the void fraction and tortuosity factor inside the catalyst particle [26,28].

3.2. Catalyst effectiveness (η)

The obtained D_{eff} value was used to compute the catalyst effectiveness, η, of the particles. The effectiveness was computed numerically using the diffusion-reaction equation [26,28]:

$$\frac{1}{r^2}\frac{d}{dr}\left(r^2 D_{eff}\frac{dC_{AB}}{dr}\right) = k\rho_s \frac{K_0 \exp((\Delta H_{ads}/RT_0) - (\Delta H_{ads}/RT))C_{AB}}{1 + K_0 \exp((\Delta H_{ads}/RT_0) - (\Delta H_{ads}/RT))C_{AB}} \tag{11}$$

Along with the BCs:

$$\begin{aligned} &\text{at } r = \frac{d_p}{2}, \quad C_{AB} = C_{AB,b} \\ &\text{at } r = 0, \quad \frac{dC_{AB}}{dr} = 0 \end{aligned} \tag{12}$$

A finite volume discretization yielded the concentration profile across the catalyst pellet which was used to compute the effectiveness factor, given by:

3.3. Pre-exponential factor (A), activation energy (E_a), adsorption energy (ΔH_{ads}) and adsorption equilibrium constant (K_0)

The LH kinetic model, as described by Eq. (2), and a nonlinear fitting algorithm [15] based on Powell's conjugate error minimization method [29], were used to obtain the kinetic parameters (A, E_a, K_0, ΔH_{ads}). Eq. (2) was discretized using a predictor-corrector finite difference scheme. The rate constants (k) at the four temperatures were initially guessed and refined iteratively by minimizing the differences between model calculations and experimental data. The catalyst effectiveness (η) was computed, with the changing bulk concentration of AB solution at each time instant and temperature, by solving the concentration profile inside the catalyst pellets using Eqs. (11)–(13) as explained in Section 3.2. The current iterate values of k, K_0 and ΔH_{ads}, the measured D_{eff} value, and the instantaneous bulk concentration of AB solution ($C_{AB,b}$) were used in Eq. (13). The variation of D_{eff} with temperature [24] was approximated, with T_{ref} = 26 °C, as:

$$D_{eff}(T) = D_{eff}(T_{ref})\left(\frac{T}{T_{ref}}\frac{\mu_{w,ref}}{\mu_w}\right) \tag{14}$$

The viscosity values, μ_w, were adopted from the thermo-physical property tables of saturated water. Powell's method and Brent's line minimization algorithm were used to determine the two unknowns, K_0 and ΔH_{ads} [15]. The parameters, A and E_a, were obtained from an Arrhenius plot using the optimized values of the rate constants. The converged values of the kinetic parameters and D_{eff} were used to re-model the reactions based on LH kinetics in the diffusion-controlled regime using Eqs. (2)–(4), to verify if η also conformed to its analytical expression shown in Eq. (3). The value of D_{eff} was refined, if needed, to match the experimental measurements and the parameters (A, E_a, ΔH_{ads}, K_0) re-assessed. As shown in Fig. 3, the obtained kinetic and diffusion parameters for the LH model, as given by Eqs. (3) and (4), and those for the nth order kinetic model as described by Eq. (8), both gave good fits to the data even though the nth order kinetic model was only intended to provide initial guesses for the LH model optimization.

3.4. Validation of obtained parameters: packed-bed reactor modeling

The obtained kinetic and diffusion parameters were validated by using them as inputs to an adiabatic, horizontal packed-bed AB hydrolysis reactor model and comparing the model results with measurements. Heterogeneous AB (5 wt%) hydrolysis, as shown in Eq. (1), in the cylindrical reactor, packed with 3 wt% cylindrical Ru/C pellets (2 mm diameter, 3 mm length), was modeled. The simulation was based on the LH kinetic model, as shown in Eq. (2), and it estimated the axial variation of temperature, species concentrations and their molar flow rates for given reactor dimensions, bulk and pellet catalyst density, and void fraction. A one-dimensional packed-bed plug-flow reactor model based on the same experimental arrangement and used for simulating SBH

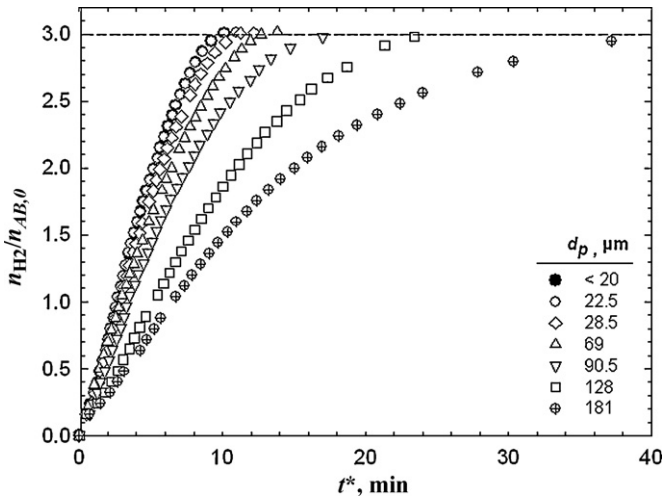

Fig. 2. Hydrogen evolution profiles at different catalyst particle sizes. Reaction conditions: $T = 26\,^{\circ}C$, $V_{sol} = 9.9$ mL, $C_{AB,0} = 260$ mol m^{-3}.

Table 1
Observed initial reaction rates at 26 °C and varying catalyst sizes.

d_p (μm)	$r_{obs} = d(n_{H_2}/n_{AB,0})/dt$ (min^{-1})
<20	0.35
22.5	0.35
28.5	0.31
69	0.27
90.5	0.23
128	0.16
181	0.11

Table 2
Converged values of the diffusion coefficient at various catalyst particle sizes at 26 °C.

d_p (μm)	D_{eff} (m^2 s^{-1})	rms error (%) of the fit
90.5	1.67×10^{-10}	2.2
128	1.60×10^{-10}	4.6
181	1.67×10^{-10}	2.1

hydrolysis [25] was modified and employed in the present study. The multi-component two-phase flow inside the reactor comprised AB, the hydrolysis by-product, and water in the liquid phase, with hydrogen and water vapor making up the gas phase. Transport phenomena involved mass and heat transfer due to convection, and mass diffusion of the adsorbed NH_3BH_3 species inside the pores of the catalyst pellets [25]. The insulated stainless steel reactor was 2.09 cm in diameter and 28.7 cm long with 10 uniformly spaced thermocouples located along its length to measure the axial temperature distribution. The experimental details of the reactor and other components in the hydrogen generation system are reported in Ref. [30]. The inlet and outlet fluid mixture densities (ρ_{in}, ρ_{out}), stoichiometric coefficients, inlet species concentrations of the different reaction components, kinetic parameters (A, E_a, K_0, ΔH_{ads}, D_{eff}), heat of reaction (ΔH_{rxn}), and inlet temperature of the AB solution were introduced in the model such that it simulated 5 wt% AB hydrolysis inside the reactor with the aqueous solution flowing in at 23 mL min^{-1}. The measured values of 978 kg m^{-3} [20] and 943 kg m^{-3} were used for the inlet and outlet liquid phase densities. The estimated value of D_{eff}, obtained as explained in Section 3.1 and Eq. (13), was used. The catalyst effectiveness was computed using relations similar to Eqs. (11)–(13) with the shape of the pellet being cylindrical. The incoming AB solution had a concentration of 1.7 kmol m^{-3} and an inlet temperature of 23 °C. The bulk catalyst density in the bed and catalyst pellet density were measured to be 570 and 656 kg m^{-3}, respectively, leading to a void fraction of 0.131. The water vapor mass transfer coefficient (k_{H_2O}) was required while accounting for the water vapor produced due to evaporation from liquid phase to the bulk gas stream [25]. Since the liquid flow rate in the present study is similar to that used previously [25], the same k_{H_2O} value of 3 m^{-1} was used. A measured pressure difference of 0.11 bar [20], across the reactor, was used. The energy, momentum and species equations were solved for the addressed initial-value problem [25].

4. Results and discussion

4.1. Effective mass diffusion coefficient (D_{eff})

AB was hydrolyzed at 26 °C and at catalyst particle sizes of 22.5, 28.5, 69, 90.5, 128 and 181 μm, as shown in Fig. 2. The observed initial reaction rates at the different catalyst sizes are listed in Table 1. The rates at catalyst sizes of 90.5, 128 and 181 μm conformed to Eq. (9), thus these reactions were in the strong pore-diffusion regime. The reactions at catalyst sizes of 22.5 and <20 μm were found to be in the kinetic-controlled regime, as seen in Figs. 1 and 2. An intrinsic reaction order of $n = 0.2$ yielded the best linear fits in the kinetic-controlled and strong pore-diffusion regimes, with the mean regression coefficient (R^2_{max}) equal to 0.9842. The slope of the $(C_{AB,0}^{1-n} - C_{AB}^{1-n}/1-n)$ versus t curve for $n = 0.2$, at the catalyst size (22.5 μm) in the kinetic-controlled regime, yielded the intrinsic rate constant (k) to be 7.1 mol^{1-n} m^{3n} kg^{-1} min^{-1}.

The reactions in the strong pore-diffusion regime at catalyst sizes of 90.5, 128 and 181 μm were modeled to obtain the value of D_{eff} at 26 °C using Eq. (8), the intrinsic values of k and n, and a predictor-corrector finite difference discretization. For each of the three cases, a guessed value of D_{eff} resulting in the least rms error between the computed and experimental $C_{AB}(t)$ values was selected. Table 2 lists the optimized values of D_{eff} (26 °C) and total rms errors obtained for the three cases, where it can be seen that D_{eff} does not vary with catalyst size. An averaged value of 1.67×10^{-10} m^2 s^{-1} was selected for the effective mass diffusion coefficient (D_{eff}).

The results of the diffusion-controlled reactions, modeled using Eq. (8), are compared with experimental data shown as dashed lines in Fig. 3. Assuming typical values for the void fraction ($\varepsilon = 0.4$)

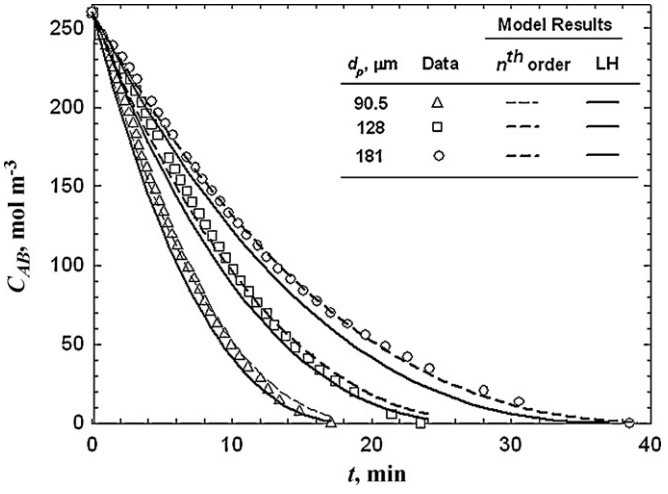

Fig. 3. Experimental data and model results in the diffusion-controlled regime at 26 °C using: (i) nth order kinetics (dashed lines) with $D_{eff} = 1.67 \times 10^{-10}$ m^2 s^{-1}, and (ii) LH kinetics (solid lines) with $D_{eff} = 2 \times 10^{-10}$ m^2 s^{-1}.

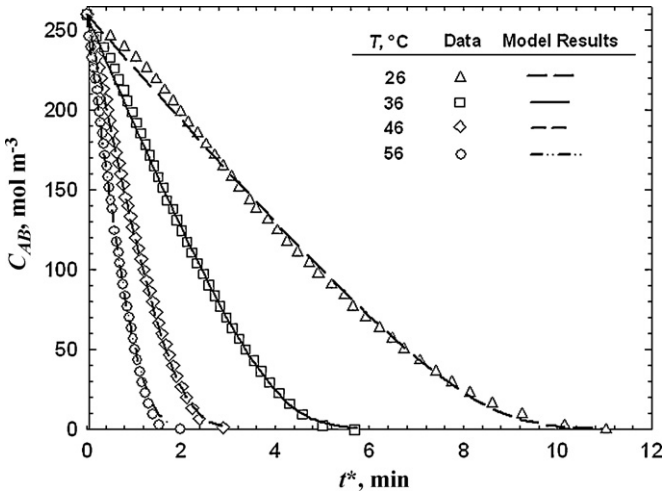

Fig. 4. C_{AB} vs t data and model results, at the four temperatures (26–56 °C), using the fitted kinetic parameters and D_{eff}.

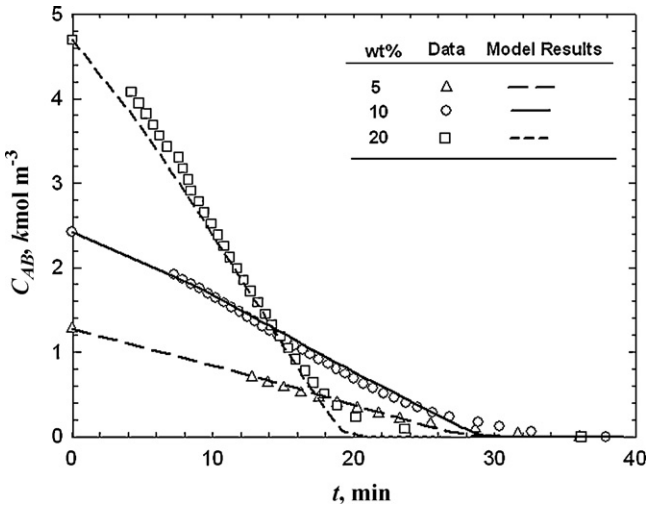

Fig. 5. Experimental data and model results for hydrolysis of concentrated AB (5–20 wt%) solutions, using kinetic and diffusion parameters estimated under dilute AB conditions.

and tortuosity factor ($\tau = 4$) in a catalyst particle [31], the bulk liquid phase diffusivity (D_l) was estimated to be 1.67×10^{-9} m^2 s^{-1}, which is in the typical range of diffusion coefficients for liquids [27]. The order of magnitude of the obtained diffusion coefficient was also verified using the Wilke–Chang correlation for estimating diffusion coefficients in binary liquid systems [32]. The diffusion coefficients at the other three temperatures of 36, 46 and 56 °C were determined using Eq. (14).

4.2. Kinetic parameters – A, E_a, K_0, ΔH_{ads}

The measured kinetic data at the four temperatures, at a catalyst size of 22.5 μm, is shown in Fig. 1. The procedure described in Section 3.3 was used to obtain the intrinsic parameters (A, E_a, K_0, ΔH_{ads}). The catalyst effectiveness, η, at the temperatures (36–56 °C) and different time instants were computed using Eqs. (11)–(13) and the current iterate values of the rate constant (k), adsorption equilibrium constant (K), and instantaneous bulk concentration of AB ($C_{AB,b}$). The η value was kept at unity at 26 °C, as suggested by the experiments (Fig. 1). The converged and optimized values of the kinetic parameters and D_{eff} were used in Eqs. (2)–(4) to model the three reactions in the diffusion-controlled regime. A refined value of 2×10^{-10} m^2 s^{-1} for D_{eff} was found to match the experimental measurements well. The procedure to obtain the parameters (A, E_a, K_0, ΔH_{ads}) was repeated, as noted in Section 3.3, using this optimized value of D_{eff}. The converged and optimized values of the four kinetic parameters and the effective diffusion coefficient in the rate equation are: $A = 1.36 \pm 0.61 \times 10^{10}$ mol (kg-cat)$^{-1}$ s^{-1}, $E_a = 60.4 \pm 1$ kJ mol^{-1}, $K_0 = 47.2 \pm 4.8$ m^3 kmol^{-1}, $\Delta H_{ads} = -32.53 \pm 2.6$ kJ mol^{-1}, $D_{eff} = 2 \times 10^{-10}$ m^2 s^{-1} with a reference temperature (T_0 in Eq. (4)) of 299 K. The overall rms error between the measured and predicted C_{AB} values versus time at all four temperatures was 1.46% of the initial concentration of the AB solution ($C_{AB,0}$). A sensitivity analysis of the fit to individual variation of each parameter showed that changes of 20% in K_0 or A, or 5% in E_a or ΔH_{ads}, produced easily observed degradation of the fits suggesting reasonable error bounds for the reported parameters. The measured and predicted C_{AB}-t values are shown in Fig. 4, demonstrating a good match.

Further, the obtained parameters were used, along with LH kinetics, to predict C_{AB}-t values for the three catalyst sizes (90.5, 128 and 181 μm) at 26 °C in the diffusion-controlled regime. The model results, shown as solid lines in Fig. 3, show a satisfactory match with the experimental measurements. Thus, the obtained kinetic and diffusion parameters can be used with confidence to predict the reaction performance with LH kinetics for variations of both catalyst particle size and temperature.

4.3. Model and parameter validation

As described above, the kinetic and diffusion parameters were obtained for dilute AB (1 wt%) solutions in a small batch reactor. In this section, we examine the applicability of these parameters, with no further adjustment, for higher AB concentrations and in a continuous-flow packed-bed reactor.

4.3.1. Hydrolysis for higher AB concentrations in a batch reactor

Hydrogen evolution measurements from the hydrolysis of concentrated AB (5–25 wt%) solutions have been reported in Ref. [20]. Non-isothermal, concentrated AB hydrolysis was modeled in the present work using the parameters (D_{eff}, A, E_a, K_0 and ΔH_{ads}) obtained under dilute conditions (1 wt%) and Eq. (2). The temperature (T), in Eq. (2), was the measured instantaneous temperature reported in Ref. [20]. The instantaneous solvent volume ($V_{sol}(t)$) was calculated by accounting for the water consumption during hydrolysis. The catalyst effectiveness was found numerically as explained in Section 3.2. A catalyst size of 22.5 μm, used in the experiments [20], was utilized for the calculations. The variations of C_{AB} with time were predicted for AB (5, 10 and 20 wt%) hydrolysis. As can be seen in Fig. 5, the model calculations match the experimental data well for all the investigated cases.

4.3.2. Continuous-flow packed-bed reactor (0.5 kW)

As described in Section 3.4, the axial temperature profile in a continuous-flow packed-bed reactor was measured for 5 wt% AB hydrolysis [20], and the experimental data are shown in Fig. 6. Using the reactor model also described in Section 3.4, we calculated the temperature profile using the kinetic and diffusion parameters obtained in Section 4.2. As shown in Fig. 6, the model calculations matched well with the experimental data. The slight mismatch near the reactor inlet may be attributed to experimental uncertainties and model limitations, also observed in Ref. [25]. The hydrogen production output rating of the reactor, 0.5 kW, was calculated using the hydrogen flow rate at the reactor outlet (~2.4 SLPM) and the low heating value of H_2 (−242 kJ mol^{-1}).

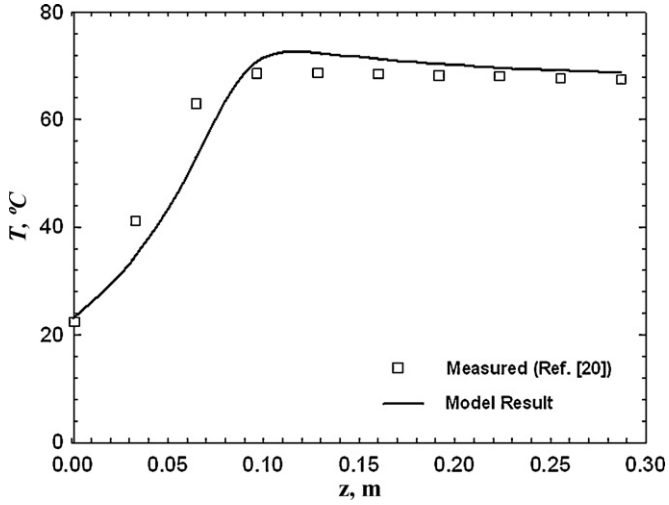

Fig. 6. Axial temperature variation for AB (5 wt%) hydrolysis along the continuous-flow packed-bed reactor – experimental data and model results. Flow conditions: $C_{AB,in}$ = 1.71 kmol m^{-3}, T_{in} = 23 °C, P_{in} = 112 kPa and P_{out} = 101 kPa.

5. Concluding remarks

In the present work, dilute AB hydrolysis (1 wt%), in a 10 mL batch, was conducted for different catalyst particle sizes and reaction temperatures. Including the catalyst effectiveness in the LH kinetic model, the intrinsic kinetic parameters and effective AB diffusion coefficient were obtained from the diffusion-influenced rate data. Further, using the parameters obtained under dilute conditions (1 wt%), AB hydrolysis at higher concentrations (5–20 wt%) in a batch reactor and also in a continuous-flow packed-bed reactor (0.5 kW) was simulated. The model results matched the experimental data well.

Acknowledgements

This research was supported by the US Department of Energy under the contract Number DE-FC36-06GO86050 with David Peterson, Jim Alkire and Katie Randolph serving as Project Officers and Carole Read and Grace Ordaz serving as Technology Managers.

References

[1] M. Gutowski, T. Autrey, Chem. World 3 (2006) 44–48, http://www.rsc.org/chemistryworld/Issues/2006/March/HydrogenOnBoard.asp.
[2] R.V. Helmolt, U. Eberle, J. Power Sources 165 (2007) 833–843.
[3] R.K Ahluwalia, J.K. Peng, J. Hydrogen Energy 33 (2008) 4622–4633.
[4] J.S. Zhang, W.N. Delgass, T.S. Fisher, J.P. Gore, J. Power Sources 164 (2007) 772–781.
[5] M.D. Riktor, M.H. Sørby, K. Chlopek, M. Fichtner, F. Buchter, A. Züttel, B.C. Hauback, J. Mater. Chem. 17 (2007) 4939–4942.
[6] PHYSORG, General Science/Chemistry, Pellets of Power Designed to Deliver Hydrogen for Tomorrow's Vehicles, 2007, http://www.physorg.com/news106920683.html.
[7] G. Wolf, J. Baumann, F. Baitalow, F.P. Hoffmann, Thermochim. Acta 343 (2000) 19–25.
[8] A.T-. Raissi, Thermoeconomic Analysis of Area II, Hydrogen Production - Part II, Proceedings of the 2002 U.S. DOE Hydrogen Program Review, NREL/CP-610-32405.
[9] A. Gutowska, L. Li, Y. Shin, C.M. Wang, X.S. Li, J.C. Linehan, R.S. Smith, B.D. Kay, B. Schmid, W. Shaw, M. Gutowski, T. Autrey, Angew. Chem. Int. 44 (2005) 3578–3582.
[10] N. Mohajeri, A.T. Raissi, O. Adebiyi, J. Power Sources 167 (2007) 482–485.
[11] P.V. Ramachandran, P.D. Gagare, Inorg. Chem. 46 (2007) 7810–7817.
[12] M. Chandra, Q. Xu, J. Power Sources 159 (2006) 855–860.
[13] M. Chandra, Q. Xu, J. Power Sources 156 (2006) 190–194.
[14] Q. Xu, M. Chandra, J. Power Sources 163 (2006) 364–370.
[15] S. Basu, A. Brockman, P. Gagare, Y. Zheng, P.V. Ramachandran, W.N. Delgass, J.P. Gore, J. Power Sources 188 (2009) 238–243.
[16] M. Chandra, Q. Xu, J. Power Sources 168 (2007) 135–142.
[17] M. Diwan, V. Diakov, E. Shafirovich, A. Varma, J. Hydrogen Energy 33 (2008) 1135–1141.
[18] S. Hausdorf, F. Baitalow, G. Wolf, F.O.R.L. Mertens, Int. J. Hydrogen Energy 33 (2008) 608–614.
[19] B.L. Davis, D.A. Dixon, E.B. Garner, J.C. Gordon, M.H. Matus, B. Scott, F.H. Stephens, Angew. Chem. 48 (2009) 6812–6816.
[20] A.C. Brockman, Ammonia Borane Hydrolysis Based Hydrogen Storage: Engineering Considerations, M.S. thesis, Purdue University, West Lafayette, May 2008.
[21] B.S. Richardson, J.F. Birdwell, F.G. Pin, J.F. Jansen, R.F. Lind, J. Power Sources 145 (2005) 21–29.
[22] A.T. Raissi, Proceedings of the 2002. U.S. DOE Hydrogen Program Review, Thermoeconomic Analysis of Area II, Hydrogen Production - Part II, NREL/CP-610-32405.
[23] R. Kumar, L. Verduzco, Hydrogen Storage Systems Analysis Working Group Meeting, Summary Report, 2006 (2007) 4–5.
[24] H.S. Fogler, Elements of Chemical Reaction Engineering, Prentice-Hall, New Jersey, 1986, Chapter 11, pp. 563–574.
[25] J.S. Zhang, Y. Zheng, J.P. Gore, I. Mudawar, T.S. Fisher, J. Power Sources 170 (2007) 150–159.
[26] G.F. Froment, K.B. Bischoff, Chemical Reactor Analysis and Design, 2nd edition, John Wiley & Sons, New York, 1990, pp. 125–197.
[27] P.B. Weisz, Chem. Eng. Prog. Symp. Ser. 25 (1959) 29–36.
[28] R. Aris, The Mathematical Theory of Diffusion and Reaction in Permeable Catalysts, vol. I, Clarendon, Oxford, 1975.
[29] R.P. Brent, Algorithms for Minimization without Derivatives, Dover, New York, 2002.
[30] J.S. Zhang, Y. Zheng, J.P. Gore, T.S. Fisher, J. Power Sources 165 (2007) 844–853.
[31] C.N. Satterfield, Mass Transfer in Heterogeneous Catalysis, MIT Press, Cambridge, 1970.
[32] R.C. Reid, J.M. Prausnitz, T.K. Sherwood, The Properties of Gases and Liquids, 3rd edition, McGraw Hill, New York, 1977, Chapter 11, pp. 544–601.